Array Phase Center Dynamics Using Spatial Amplitude Modulation for High Efficiency Secure Wireless Communication

Jacob R. Randall, *Graduate Student Member, IEEE,* Jason M. Merlo, *Graduate Student Member, IEEE,* Amer Abu Arisheh, *Graduate Student Member, IEEE,* and Jeffrey A. Nanzer, *Senior Member, IEEE*

***Abstract*—We present an approach to secure wireless communication based on dynamically changing the apparent phase center of a two-element antenna array using spatial amplitude dynamics. We implement phase center dynamics by modulating the relative amplitudes of the signals fed to two antenna elements. By moving the phase center symmetrically with respect to the geometric center of the array, the far-field amplitude pattern remains mostly constant while the phase pattern changes, imparting modulation onto the transmitted or received signals that is a function of angle. The resulting directional modulation effectively scrambles the information in the radiated waveform at angles outside of the information beam, where the modulation impacts are negligible. The result is a narrow region where information is recoverable, and since the radiated power does not change, the efficiency remains high. We present the design of a 2.5 GHz two-element array with asymmetric amplitude modulation and characterize the phase center location as a function of the amplitude ratio between the elements. We demonstrate secure wireless communication experimentally in a high signal-to-noise ratio (SNR) environment, demonstrating the reduction in throughput due solely to the phase center dynamics. Finally, we analyze the information beamwidth and present a design procedure relating the amplitude ratio, SNR, element spacing, and QAM modulation format to the information beamwidth.**

***Index Terms*—Directional modulation, dynamic antennas, dynamic arrays, phase center**

I. Introduction

Security is becoming an increasingly important aspect of wireless communications as the number of network devices rapidly increases, making intentional or unintentional interference between systems more likely. Whereas traditional security approaches relying on encryption of the information generated at baseband remains crucial, there is increasing interest in applying additional security techniques at the physical layer. Physical layer security approaches have the potential to be applied in a way that is effectively separate from the underlying information, providing an approach that is transparent to the larger communication system and that can be applied to existing as well as future system architectures. When implemented at the aperture in particular, physical layer security can be implemented in an angle-dependent manner such that the signal encryption is unique at all angles. Directional modulation (DM) is a technique that imparts such encryption through modulation of the antenna radiation pattern in amplitude and/or phase at angles outside of a desired information beam. Thus, while energy may be transmitted over a wide angular range, the recoverable information is constrained to a narrow information beam, the width of which can be far narrower than the beamwidth of the power pattern.

Directional modulation has been implemented using a range of antenna techniques. Array-based DM approaches have been implemented, which rely on modulating the phase weights of the elements [1]–[3], by switching subsets of antennas on and off [4], [5], or by switching the feed between two antennas in a two-element array in an on/off keyed (OOK) approach [6]. While these approaches are able to generate DM, the approaches generally result in reduced gain since the aperture is not efficiently utilized. Other approaches have sought to implement DM using switching schemes to maximize the bit-error ratio (BER) in undesired directions by combinatorial interference [7] based on using vector synthesis analysis of DM transmitter designs [8]. However, these methods require complicated antenna architectures that are electrically large and may not be feasible in all applications. Other approaches include near-field parasitic element switching to implement DM [9]. Modeling of such systems is complex, and typically their characterization requires rigorous calibration to determine a lookup table of states that correspond to given directions. To overcome the reduction in efficiency that generally accompanies DM implementations, a dynamic distributed array was implemented in [10] where, using the additional degree of freedom of element motion, DM was implemented while maintaining maximum transmit power at all times. However, this approach relied on platform motion, which may be a limiting factor to secure high data rates. Demonstrating directional modulation within a small aperture has also been investigated at the single element level using a simple dipole architecture [11], and with arrays of electrically small antennas [12]. Other compact structures use stacked patch antennas to excite different modes [13].

In this work, we present a new approach to achieving high-efficiency DM that synthesizes the motion of the electrical location (phase center) of the transmitter using spatial amplitude dynamics. By dynamically changing the relative amplitudes of the signals fed to a two-element antenna array while keeping the array power constant and relative

This work was supported in part by the National Science Foundation under Grant #2028736. *(Corresponding author: Jeffrey A. Nanzer)*

The authors are with the Department of Electrical and Computer Engineering, Michigan State University, East Lansing, MI 48824 USA (email: randa130@msu.edu, merlojas@msu.edu, abuarish@msu.edu, nanzer@msu.edu).

phases equal, a dynamic phase pattern is implemented while the amplitude pattern of the array remains largely constant. In contrast to OOK arrays, we show that using an amplitude ratio between a traditional 50/50 split used in typical two-element arrays and a 100/0 split (used in OOK) achieves effectively the same radiated power, gain and efficiency while the OOK approach yields significantly reduced gain. We characterize the motion of the phase center of the antenna both numerically and through measurements using established phase center estimation techniques [14], and demonstrate that by changing the amplitude ratio between the two elements, the phase center of the antenna moves, synthesizing electrical motion of the antenna, which leads to dynamics in the radiated phase pattern. While our recent work demonstrated the design of an asymmetric power divider providing a single amplitude ratio [15], in this work we present experimental results of a 2.5 GHz antenna with four different relative amplitude ratios, demonstrating the ability to obtain a narrow information beam. Furthermore, experiments were conducted with high signal-to-noise ratio (SNR), such that all errors obtained outside the information beamwidth are due solely to the antenna dynamics, and not due to reduced SNR. Finally, we present a detailed characterization of the information beam and obtain a formula for determining the information beamwidth in terms of the amplitude ratio, the separation between the antennas, SNR, and the QAM constellation format.

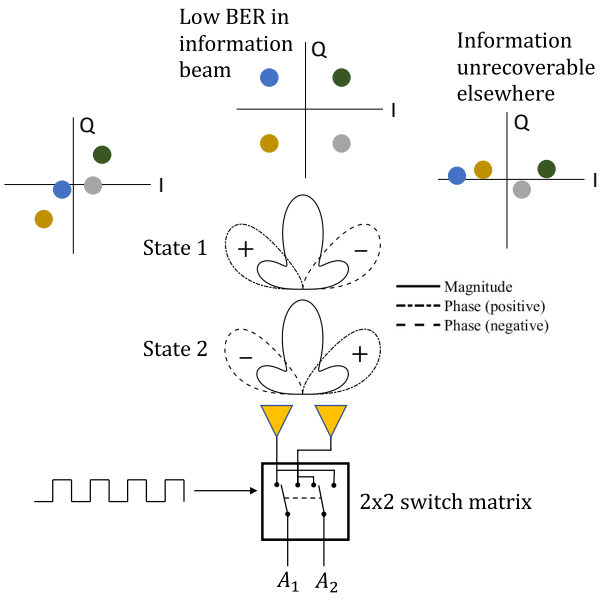

Fig. 1: The dynamic array rapidly switches two amplitude-asymmetric inputs between the two antenna feeds. The magnitude of the radiation pattern remains constant between the two states; however, the phase patterns undergo a sign flip. This generates an angle-dependent phase modulation onto the pattern that is negligible at broadside but prominent at angles away from broadside. Information transmitted or received away from broadside undergoes additional modulation due to the phase modulation imparted by the dynamic pattern, making the information unrecoverable and generating a narrow information beam near broadside. The information beam can be steered using additional complex signal weighting.

II. Dynamic Antenna Theory and Design

A. Theory

The dynamic phase center antenna is based on rapidly switching the relative amplitudes of the signals fed to two antennas. In the far field, the electric field intensity of an array of two identical elements with different currents is given by

$$\mathbf{E}(\mathbf{r}) = jk\eta \frac{e^{-jkr}}{4\pi r} \mathbf{a}(\theta,\phi)\, AF(\theta,\phi) \tag{1}$$

where $k = 2\pi/\lambda$ is the wavenumber, η is the impedance of the medium, and

$$\mathbf{a}(\theta,\phi) = \int_V \mathbf{J}(\mathbf{r}')\, e^{jk\hat{\mathbf{r}}\cdot\mathbf{r}'} dV' \tag{2}$$

is the element pattern where $\mathbf{J}$ is the normalized current density, assumed to be equal on each antenna, and the antenna extends over the volume V. Primed coordinates refer to the locations of the sources, while unprimed coordinates refer to locations of the fields. The term

$$AF(\theta,\phi) = \sum_{i=1,2} \frac{I_i}{I_0} e^{jkx_i \cos\phi} \tag{3}$$

is the array factor which accounts for different weighting of the antenna currents through the terms $\frac{I_i}{I_0}$, where I_0 is a nominal reference current. The driving signals to each antenna can then be characterized as a current given by

$$I_i = w_i I_o \tag{4}$$

where w_i is a complex weighting factor on each current, which can be defined for a desired beamsteering angle, for example.

This work considers the use of differential amplitude weighting to impart directional modulation. The differential amplitude weights may be applied in addition to the complex weights w_i, thus we can write the drive currents as

$$I_i' = A_i I_i \tag{5}$$

We consider the antenna weights to be asymmetric, and to switch the signals between two states with a given periodicity. The weights can be thus given as

$$\begin{aligned} A_1 &= \alpha(t) \\ A_2 &= 1 - \alpha(t) \end{aligned} \tag{6}$$

where

$$\alpha(t) = \begin{cases} a, & (n-1)\,T_0 < t < \left(n - \frac{1}{2}\right) T_0 \\ 1-a, & \left(n - \frac{1}{2}\right) T_0 < t < nT_0 \end{cases} \tag{7}$$

in which $0 \leq a \leq 1$, T_0 is a period over which the antenna switches between the two states, and n is an integer. The two states thus consist of the same two drive currents, but they are switched between the two antennas, mirroring the drive current weights at each antenna. The differential weighting can be characterized in terms of the amplitude ratio $\chi = 20\log_{10}[\frac{a}{1-a}]$. In this work, we consider the ratios ± 0 dB, ± 6 dB, ± 12 dB, and $\pm\infty$ dB. The ± 0 dB case is equivalent to a standard array with equal amplitude weighting at each element, while the $\pm\infty$ dB case is equivalent to an OOK scheme, where only one antenna is driven at a time in each state.

Switching the amplitudes between the two symmetric states results in a far-field amplitude pattern that is unchanged, while the phase pattern is mirrored. For a two-element array aligned along the x-axis, centered at the origin, and with weights $w_i = 1$, the array factor reduces to

$$AF(\phi) = A_1 e^{-jk\frac{d}{2}\cos\phi} + A_2 e^{jk\frac{d}{2}\cos\phi} \tag{8}$$

where $d = |x_2 - x_1|$ is the separation of the antennas. The magnitude of the array factor is

$$|AF(\phi)| = \left[A_1^2 + A_2^2 + A_1 A_2 \cos\left(kd\cos\phi\right)\right]^{-\frac{1}{2}} \tag{9}$$

and the phase is

$$\angle AF(\phi) = \tan^{-1}\left[\left(\frac{A_2 - A_1}{A_1 + A_2}\right)\tan\left(\frac{kd}{2}\cos\phi\right)\right] \tag{10}$$

When the antenna driving currents are swapped, i.e. $A_1 \to A_2$ and $A_2 \to A_1$, the magnitude (9) is unchanged. The phase (10), however, undergoes a sign change at all angles except $\phi = 90°$, thus creating a phase differential in the radiation pattern away from the broadside direction when the inputs are swapped, while keeping the magnitude the same. This is illustrated in Fig. 1. By switching rapidly between these two states, phase modulation commensurate with the differential phase will be imparted on the signals transmitted or received by the array. The region where this modulation is sufficiently small such that the information is recoverable is referred to as the information beam. In Section V we characterize the beamwidth of this region. Note that the information beam can be steered by modifying the complex weights w_i.

B. Antenna Design

A two-element microstrip patch antenna array was built at 2.5 GHz to evaluate the concept. The antenna was fabricated on Rogers 4350b with a thickness of 1.542 mm. The antennas each had a length of 29.95 mm and a width of 39.28 mm [16]. The length of the ground plane and substrate have an additional $\frac{\lambda}{4}$ or greater spacing for a total length of 181 mm and width of 99.5 mm. The feed point was then designed to impedance match the antenna to 50 Ω which was 9.6 mm from the edge of the patch. The antenna was simulated in Ansys High Frequency Structure Simulator (HFSS), and the simulated gain was 5.74 dBi. A gain measurement of the single antenna was done in a fully enclosed anechoic chamber yielding a measured gain of 5.7 dBi at the designed frequency of 2.5GHz. The two-element array was then constructed and evaluated in HFSS, and an ideal simulation conducted in MATLAB. Source feed amplitudes were simulated with different amplitude ratios in HFSS, and the resulting magnitude and phase patterns were exported into MATLAB to compare against measured results. Two 2.5 GHz single element antennas were manufactured and placed physically 0.75λ apart as shown in Fig. 2(a) with the manufactured array shown in Fig. 2(b). This spacing was chosen to ensure the presence of high sidelobes greater than -20 dB, which in a static array would result in information transmission in directions outside the mainbeam. This also

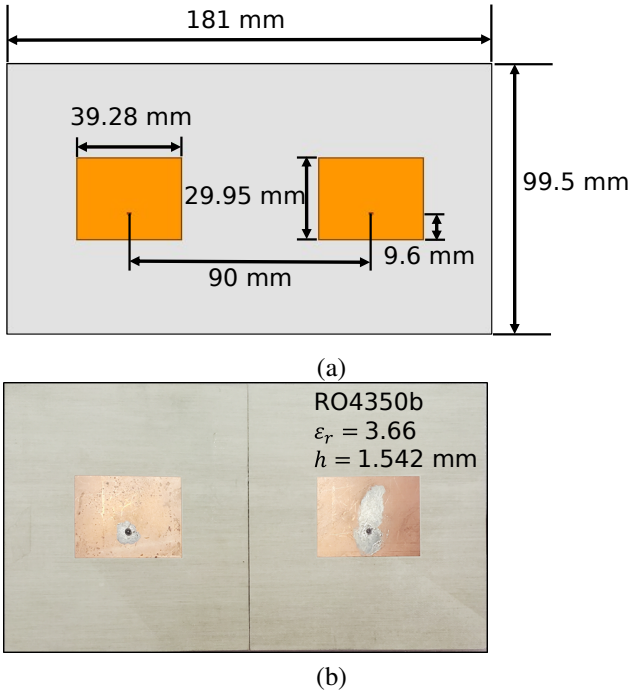

Fig. 2: Two-element microstrip patch array designed at 2.5 GHz with 0.75λ spacing. (a) HFSS model and (b) Fabricated antenna.

mitigates mutual coupling, which is most prominent up to half-wavelength element separations.

The antenna system was measured in a semi-anechoic environment using the setup shown in Fig. 3. The setup was used to characterize the differential patterns of the antennas as a function of angle and amplitude ratio, which are later analyzed to characterize the impact on BER (see Section IV). The two-element array was placed on a rotating platform and operated in receive mode. The transmitter consisted of a Keysight N5183A continuous wave signal generator connected to an L-Com HG2458-08LP-NF log-periodic antenna and was located approximately 3.61 m down range. The array was calibrated for amplitude ratios of 0 dB, 6 dB, 12 dB, and ∞ dB with a tolerance of ± 0.1 dB and a phase tolerance of $\pm 1°$ by using attenuators and cables. While the attenuators would not be used in a practical communication system due to added resistive losses in the system, here they are used as a proof of concept. A Narda 3752 precision coaxial phase shifter was used to ensure that both radiated signals were in-phase at broadside, and then the power from both radiators were combined before being received by a Keysight MSOX92004A oscilloscope. For each amplitude ratio case, two magnitude and two phase patterns (one for each state) were measured. The transmitted signal was split between the transmit antenna and a second channel on the oscilloscope, and was used to compare to the received signals to calculate the relative phase patterns of the antenna in its two states. The magnitude and phase patterns were measured from $\phi \in [-90, 90]$ in $1°$ increments. An intentionally high SNR experiment was conducted to ensure that any bit errors would be the result only of the differential array patterns, and not due to noise. The minimum SNR at broadside was approximately

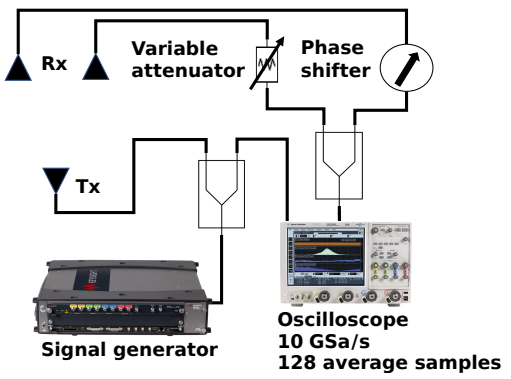

(a)

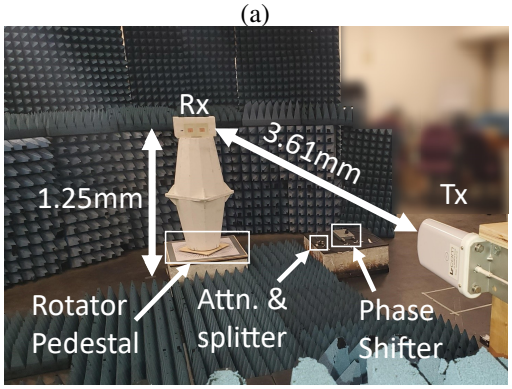

(b)

Fig. 3: Experimental test setup. (a) Block diagram of the setup. The array was set in receive mode, with the signals phase and amplitude matched to obtain the desired amplitude ratios. The cables were swapped to synthesize the two antenna states. (b) Photograph of the test setup in a semi-anechoic environment.

60 dB, with a minimum SNR of 30 dB spanning all other angles. These patterns were then imported into a simulated communication channel to model spatial pattern dynamics and communications performance (see Section IV).

The HFSS-simulated and measured magnitude and phase patterns of the array are shown in Fig. 4 for the amplitude ratio cases of $|\chi| = 0$ dB, $|\chi| = 6$ dB, $|\chi| = 12$ dB, and $|\chi| = \infty$ dB for the two states S1 and S2. The amplitude patterns remain constant between the two states regardless of χ, which matches the theoretical magnitude pattern (9). For the equal amplitude case $|\chi| = 0$ dB, which corresponds to the traditional phased array amplitude weighting, the phase pattern does not change as the states are switched. However, for $|\chi| \neq 0$ dB, the amplitude pattern undergoes a sign flip, mirroring the phase pattern across broadside. This behavior matches the theory in (10). If the array is rapidly switched between the two states, a differential phase will be modulated onto the transmitted or received signals at all angles except at broadside ($\phi = \frac{\pi}{2}$) where the phase is equal for both states. This modulation, if done at a sufficiently fast rate, will effectively scramble the information outside of a region close to broadside, making it unrecoverable. Note that the equiphase point at broadside can be steered to any angle by changing the weights w_i of the driving signals (4) in a traditional beamsteering operation.

TABLE I: Array Performance vs. Amplitude Ratio

Ratio (dB)	HPBW(°)	Gain (dB)	Eff (%)	EIRP (dBm)
0	35	9.2	80.5	15.4
6	38	8.7	81.0	15.5
12	44	7.8	81.3	15.5
∞	76	6.2	81.6	15.5

C. Array Performance Comparison

One of the challenges of implementing directional modulation in arrays involves reduced gain or efficiency when modifying the element weights. In particular, many approaches rely on switching elements off periodically or otherwise lose mainbeam gain. In a two-element array, an OOK approach will result in only a single element driven at a time, as seen by (3), which will lead to reduced gain since the added directivity of the array factor is not utilized. Furthermore, turning elements off in larger arrays without reallocating the power will lead to reduced effective isotropic radiated power (EIRP).

We consider the impact on the array half-power beamwidth (HPBW), gain, efficiency, and EIRP as a function of the amplitude ratio by simulating the array performance in HFSS. The results are given in Table I. EIRP is calculated using the total array input power of 10 dBm. The conduction and dielectric losses are approximately 0.8 dBm. In the 0 dB ratio (a 50/50 amplitude split corresponding to a typical two-element antenna array), the parameters are commensurate with a typical two-element antenna array. In the other extreme case, the ∞ dB case where only one antenna is driven at a time, the HPBW increases commensurately, and the gain reduces due to the lost array gain. Since all the signal power is now directed to one antenna, the EIRP is effectively unchanged, however the gain reduction is significant. The two cases with asymmetric but nonzero amplitudes provide more interesting results. For both the 6 dB and 12 dB cases the HPBW increases slightly, and the gain decreases slightly, while the efficiency and EIRP remain constant. In both cases, the performance is close to that of the standard two-element array. However, since the amplitude ratio is changed, the antenna phase center will also move, leading to differences in the radiated field patterns, as shown below in Section III. Thus, by implementing an asymmetric but nonzero amplitude ratio, high gain and efficiency can be maintained while supporting dynamic phase differences in the radiation patterns.

III. Dynamic Phase Center Interpretation

At angles within the mainbeam of the array, where $\phi \approx \frac{\pi}{2}$, the array factor phase (10) simplifies since at these angles the term $\cos\phi \approx \frac{\pi}{2} - \phi \ll 1$, and thus the small argument approximations $\tan\theta \approx \theta$ and $\tan^{-1}\theta \approx \theta$ can be used. The phase of the array factor is then

$$\angle AF \approx \left(\frac{A_2 - A_1}{A_1 + A_2}\right)\frac{kd}{2}\cos\phi \tag{11}$$

When the weights are defined as in (6), the phase reduces to

$$\angle AF \approx (1 - 2\alpha)\,\frac{kd}{2}\cos\phi \tag{12}$$

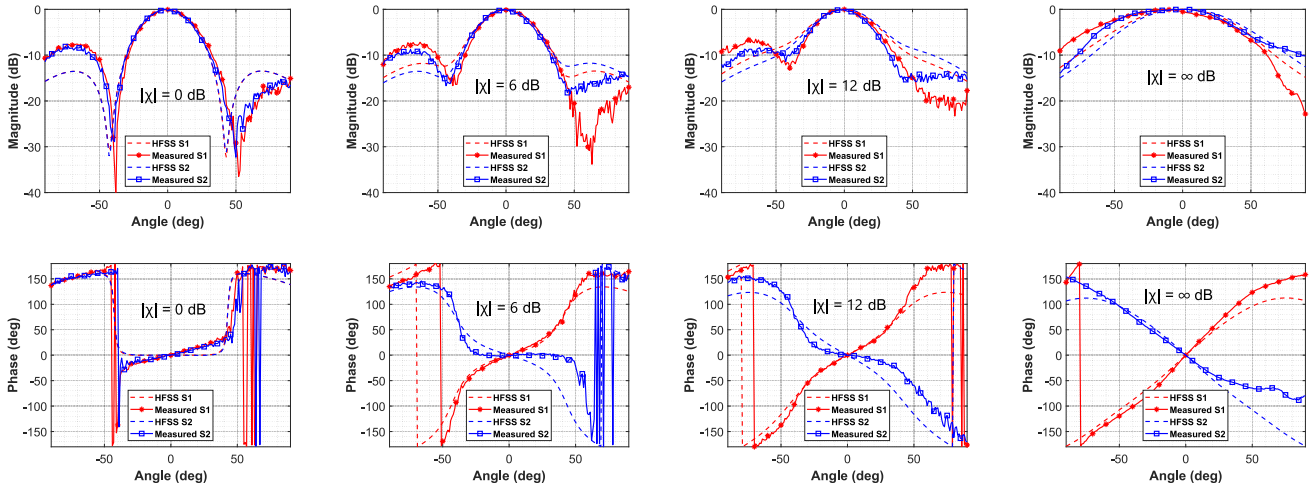

Fig. 4: Magnitude (top) and phase (bottom) patterns over observation angle $\frac{\pi}{2}-\phi$ for the two-element array for the four amplitude ratio cases of $|\chi| = 0$ dB, $|\chi| = 6$ dB, $|\chi| = 12$ dB, and $|\chi| = \infty$ dB for the two states S1 and S2. The amplitudes of the drive signals swap between S1 and S2. While the amplitude patterns remain the same between the two states, the phase patterns undergo a sign change at all angles except at broadside, and except for the 0 dB case, which corresponds to equal amplitude on each antenna (the typical array weighting). Thus, for $|\chi| \neq 0$ dB, as the antenna is switched rapidly between the two states, the transmitted or received signals are modulated by the differential time-varying phase of the patterns everywhere except at broadside. The unmodulated region near broadside may be steered by adding additional complex weights to the drive signals.

The phase is thus linearly proportional to the amplitude factor α for angles $\phi \neq \frac{\pi}{2}$. When $\alpha = 0$, the phase is $\angle AF = \frac{kd}{2}\cos\phi$; when $\alpha = 1$, $\angle AF = -\frac{kd}{2}\cos\phi$; and when $\alpha = \frac{1}{2}$ (broadside to the array), $\angle AF = 0$. Note that when $\phi = \frac{\pi}{2}$, $\angle AF = 0$ for all α.

In essence, the above indicates that the apparent electrical location of the array changes linearly as a function of α, which generates a change in the phase of the received signal that is commensurate with the change in electrical location relative to the observation point. The electrical location of the antenna is referred to as the antenna apparent phase center [17], [18]. The phase center of an antenna is an idealized point in space where radiation is emitted such that the phase is a constant over the surface of an outward radiating sphere. Since real antennas cannot support isotropic radiation [19], the phase center only corresponds to the physical location of the antenna for theoretical point radiators. The geometries of physical antennas generate complex current densities that cause the phase center to deviate from the physical location of the antenna, thus in practice the apparent phase center is considered. The apparent phase center varies with frequency, the geometry of antenna, antenna polarization, and angular position of observation.

The phase center of the two-element array can be visualized as a radiating point x_{pc} that exists between the phase centers of the two antennas. The phase center varies in position as a function of α between the locations of the two antennas, i.e.,

$$-\frac{d}{2} \leq x_{\mathrm{pc}}(\alpha) \leq \frac{d}{2} \tag{13}$$

As the phase center moves, the phase of the outgoing spherical wave ψ changes in response to the phase center location and observation angle by

$$\psi = 2\pi\frac{x_{\mathrm{pc}}}{\lambda}\cos\phi = kx_{\mathrm{pc}}\cos\phi \tag{14}$$

Comparing to (12), it can be seen that the dynamic phase center can be characterized in terms of the amplitude ratio by

$$x_{\mathrm{pc}} = (1-2\alpha)\frac{d}{2} \tag{15}$$

such that the phase of the radiation pattern is

$$\angle AF \approx \psi = kx_{\mathrm{pc}}\cos\phi \tag{16}$$

Thus, by characterizing the phase center of the antenna as a function of the amplitude ratio, the relative change in the radiation pattern phase can be determined.

Estimating the phase center of an antenna is challenging in general; however, various methods have been developed. These include the edge diffraction method [20], which is well characterized to large horns, the vector method [18], which derives an expression for the horn phase center based off the two-point method [21], and the second derivative method, which is well characterized for parabolic reflectors [17]. Other phase center determination methods are measurement-based, such as the differential phase correction method [22] and the three-antenna method [23]. Analytical solutions to determining phase center are iterative in their approach such as the weighted phase efficiency method [24], the differential phase method [25], and the mean electrical phase center (MEPC) method [14], which derives the phase center geometrically from a set of two phase pattern measurements. In this work we use the MEPC method because it operates in closed form, is not specific to the antenna geometry, and does not require significant computation. MEPC provides a cluster of phase center locations; we modify the MEPC approach by taking the mean of the cluster, and we calculate the phase center over $\pm 18°$ of the mainbeam of the array.

The phase center of the array was estimated for an ideal array consisting of two isotropic antennas modeled in MATLAB, a patch antenna array simulated in HFSS, and

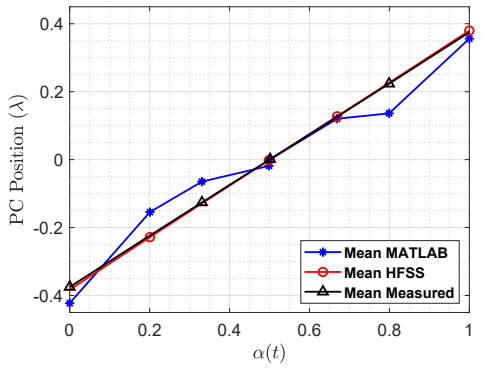

Fig. 5: Estimation of the phase center in wavelengths as a function of the amplitude ratio α for the two-element 0.75λ array. The phase center was estimated in simulation from an array of ideal isotropic radiators in MATLAB, a simulation of the patch antennas in HFSS, and from measurements of the fabricated antenna. All were based on the MEPC method [14] but modified to take the mean over an angular region of $\pm 18°$. The phase center follows a linear progression between the two extremes, which correspond to the locations of the individual antenna elements.

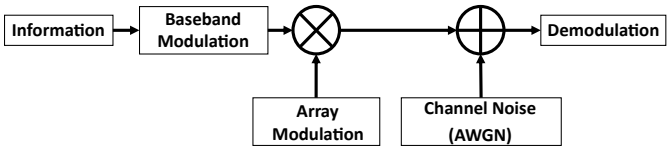

Fig. 6: Block diagram of the simulated QAM communication channel

from the measured patterns of the fabricated antenna array for the amplitude ratios ± 0 dB, ± 6 dB, ± 12 dB, and $\pm\infty$ dB. The estimation of the phase center in wavelengths using all three are shown in Fig. 5. The phase center follows a linear progression over a span of $d = 0.75\lambda$, which is the electrical spacing of the antennas, and which matches (13). At the extremes, the phase center is located at one of the two elements in the array and progresses approximately linearly between the two antennas.

IV. Secure Wireless Communication Evaluation

The communications performance of a dynamic array switching between two amplitude states was simulated in MATLAB. The complex radiation patterns for the two simulated cases (isotropic radiators simulated in MATLAB and the patch array simulated in HFSS) as well as the measured patterns from the fabricated two-element array were imported into the communications channel model shown in Fig. 6. The model generated a 48 kbit pseudo-random bit sequence that was modulated onto a 16-QAM signal using Gray coding. The array patterns were then implemented and switched between the two states at a rate equal to the symbol rate of the data, generating an angle-dependent signal. The amplitude patterns are equal for each state, but the phase patterns differ, thus the information is modulated by an additional phase modulation that is dependent on the angle as shown in (10) and (16). Additive white Gaussian noise (AWGN) was then added to yield an SNR of 40 dB. This SNR is sufficiently high to ensure that there are no bit errors from noise alone, thus any increase

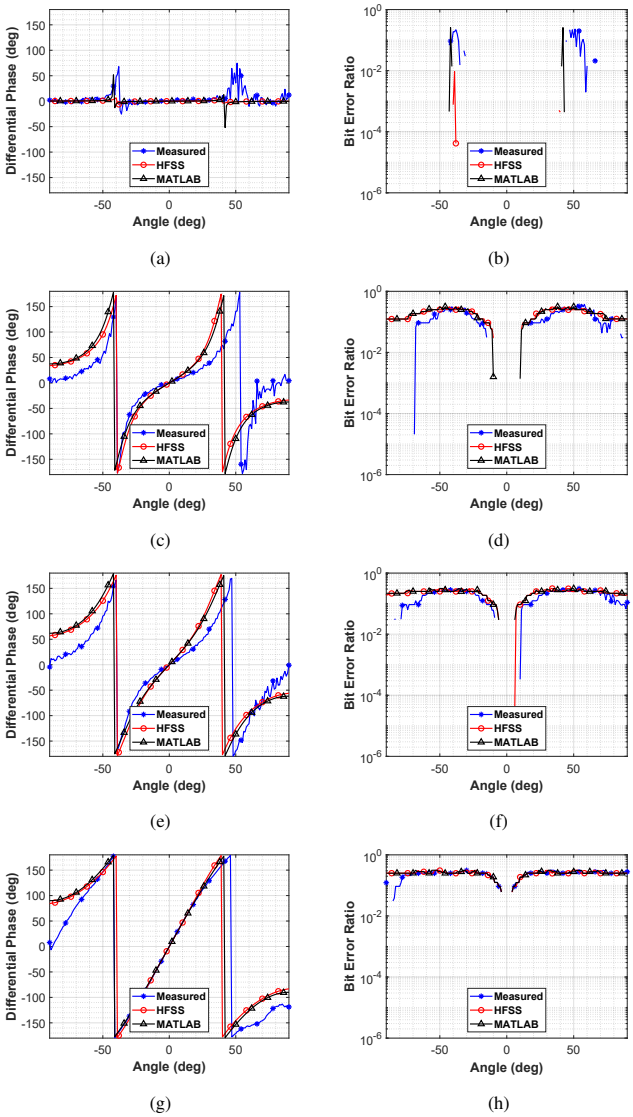

Fig. 7: Differential phase pattern (left column) and resulting BER (right column) for (a/b) $|\chi| = 0$ dB, (c/d) $|\chi| = 6$ dB, (e/f) $|\chi| = 12$ dB, and (g/h) $|\chi| = \infty$ dB for a 16-QAM signal with 40 dB SNR. The $|\chi| = 0$ dB case yields low BER at nearly all angles since the differential phase pattern is essentially zero for all angles. For other values of χ, the BER increases significantly outside of the broadside region ($\frac{\pi}{2} - \phi \approx 0$) due to the large phase differential imparted by switching between the two states. As the phase differential increases, the information beam, where the BER is low and thus the information is recoverable, narrows.

in the BER is due solely to the directional modulation added by the dynamic array. Demodulation was implemented without assuming the additional modulation due to the dynamic array pattern, after which the BER was calculated as a function of angle.

While this work analyzed the case where the switching rate and symbol rate are equal, it is reasonable to expect that the technique will be as effective if the switching rate is close to that of the symbol rate, but not exactly the same. Faster switching rates are also expected to be effective; however, an analysis of significantly slower switching rates is outside the scope of this paper. A random switching rate with mean equal to that of the symbol rate was explored through simulation,

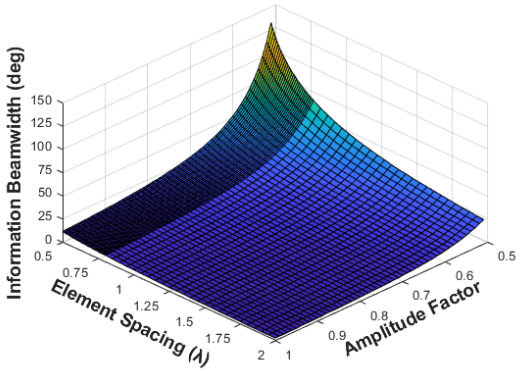

Fig. 8: Information beamwidth versus element spacing and amplitude factor a (see (7)) for 8-QAM, showing the exponentially decaying dependence with respect to both variables.

and did not show a degradation in BER compared to the periodic switching case. Different switching rates may impact performance because of spurious signals generated by the RF switch; in [15] we presented an analysis showing that such spurious signals were negligible for typical switching parameters and RF hardware.

Fig. 7 shows the differential phase patterns and resulting BER for each amplitude ratio. The differential phase pattern for the equal amplitude case $|\chi| = 0$ dB is essentially zero across all angles. This can be interpreted as the phase center remaining stationary at the centroid of the two antennas even when switching between the two states. The BER remains low across all angles; no bit errors were seen in most cases. Some errors were observed at the nulls of the beam pattern, where the amplitude approached zero and thus the noise was prominent. Outside of these narrow regions, however, the SNR was sufficiently high to result in zero bit errors.

As the amplitude ratio is changed, the differential phase pattern becomes appreciable, imparting additional phase modulation onto the information at angles away from broadside ($\frac{\pi}{2} - \phi \approx 0$). The result is a significant increase in BER due to the additional phase modulation. The region where the BER remains low is referred to as the information beam and is the angular region where the information remains recoverable. As the amplitude ratio is increased, the information beamwidth decreases, resulting in a narrower information beam, and thus a narrower region where the information is recoverable. This is despite the fact that energy is still being transmitted to all angles, as can be seen by the magnitude patterns of Fig. 4. Thus, the additional phase modulation due to dynamic switching of the array between the two states successfully impart directional modulation onto the information.

V. Information Beamwidth Model

In this section we obtain an empirical model of the angular width of the information beam, called the information beamwidth (IB), in terms of parameters of the antenna system, the information, and the SNR. The objective is to predict the spatial parameters of a secure wireless operation in terms of

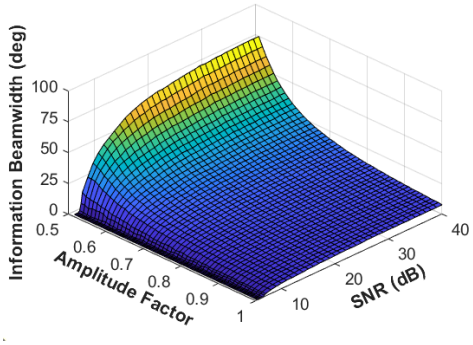

(a)

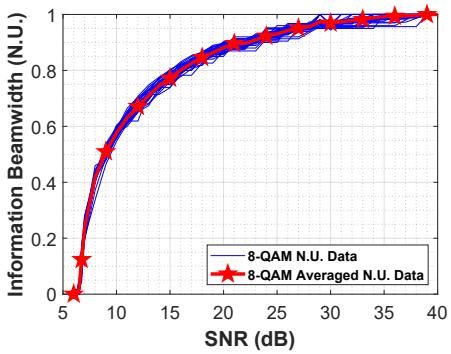

(b)

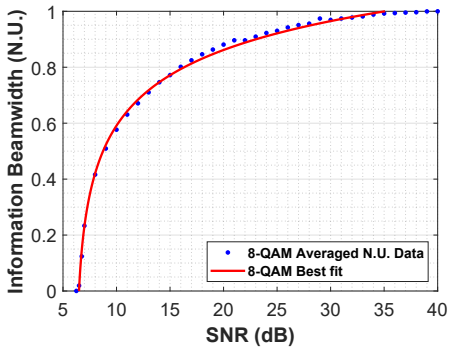

(c)

Fig. 9: Information beamwidth versus SNR and amplitude ratio with a 0.75λ element spacing transmitting 8-QAM constellation symbols. (a) 3D surface plot showing a logarithmic dependency of SNR upon the information beamwidth. (b) The normalized unit (N.U.) and averaged relationship across all amplitude ratios showing consistent effect of SNR. (c) The 2D curve fit of the averaged N.U. data shows good agreement using trust-region reflection algorithm and least absolute residuals (LAR) robustness.

the controllable aspects in a given design. We obtain a model for the information beamwidth as a function of the following parameters:

- Amplitude factor a (see (7))
- Antenna separation d
- SNR
- QAM modulation order

The IB is defined in this work as the angular separation at which BER $\leq 10^{-3}$ and that corresponds to the mainbeam of the array. The beamwidth is evaluated for isotropic radiators simulated in MATLAB assuming that the array states are

TABLE II: Information Beamwidth Model Parameters

Modulation	c_1	c_2	c_3	c_4	c_5	c_6	c_7	c_8	c_9	c_{10}
4-QAM	9.3930E1	5.2948	1.2905	45.894	2.5419	4.0641	23.257	4.1543	0.0321	-22.560
8-QAM	2.3329E1	10.788	1.2730	28.024	2.4638	2.5935	1.0049	5.3642	0.5117	-0.2251
16-QAM	1.0293E4	11.485	3.7600	8.9482	2.4549	0.8314	1.1804	4.9773	0.5000	-0.4220
32-QAM	6.4374E4	15.568	2.3447	10.545	2.4151	1.0019	0.9874	5.3609	0.5100	-0.1944
64-QAM	1.8174E5	19.700	0.6816	27.943	2.3782	2.7077	65.740	4.1961	0.0091	-64.971
128-QAM	1.1013E5	25.716	0.0161	845.74	2.3201	84.151	37.969	4.4037	0.0140	-37.169
256-QAM	1.6369E5	30.843	0.0016	6698.0	2.2877	681.49	18.939	4.3782	0.0275	-18.138
512-QAM	1.5277E8	33.088	0.4044	16.101	2.1652	1.6997	124.34	4.5742	0.0035	-123.50
1024-QAM	4.4095E5	30.932	0.0033	1241.3	1.8970	130.53	159.91	4.1395	0.0033	-159.11

TABLE III: Information Beamwidth Model Error

Modulation	RMSE (°)
4-QAM	1.22
8-QAM	1.08
16-QAM	1.15
32-QAM	1.21
64-QAM	1.27
128-QAM	1.25
256-QAM	1.15
512-QAM	1.01
1024-QAM	0.97

switched at a rate equal to the symbol rate of the information. The same communications channel model as in Section IV was used, with at 48 kbit pseudo-random bit sequence using Gray coding and an SNR of 40 dB. QAM modulation orders from 4-QAM to 1024-QAM were evaluated.

The information beamwidth was computed across a range of element spacing between $0.5\lambda \leq d \leq 0.8\lambda$ in 0.01λ increments, $0.8\lambda \leq d \leq 2.0\lambda$ in 0.05λ increments, and an amplitude factor range between $0.51 \leq a \leq 1$ in 0.01 increments. The information beamwidth was plotted versus amplitude ratio and element spacing for nine different QAM constellations ranging from 4-QAM to 1024-QAM. A 3D surface was curve fitted to the response, from which it was determined that the surface displayed an exponentially decaying relationship with respect to each variable. Fig. 8 shows the result of the information beamwidth versus element spacing d and the amplitude factor a for 8-QAM, showing the exponentially decaying dependence on both variables. Similar plots were generated for other QAM orders, each with exponentially decaying dependence, although with different specific weights, yielding an information beamwidth dependence of the form

$$\mathrm{IB}_1 = [c_1 e^{c_2 a} + c_3][c_4 e^{c_5 d} + c_6] \tag{17}$$

where c_i, $i = [1, 6]$ are coefficients that are determined empirically based on curve fitting.

Since SNR is independent of the physical array design, we consider the impact of SNR to be separable from that of the amplitude ratio and element spacing. The information beamwidth was thus characterized for $6 \leq \mathrm{SNR} \leq 40$ dB in increments of 1 dB for all QAM modulation orders and versus amplitude ratio for an element spacing of 0.75λ. The 3D surfaces were generated as a function of SNR and amplitude factor a as shown in Fig. 9(a). Each 2D curve of SNR versus the information beamwidth was individually normalized to unit data (N.U.) and plotted as shown in Fig. 9(b). The average of all normalized data was used as the reference for curve fitting. These parameters fit to a logarithmic dependence on SNR given by

$$\mathrm{IB}_2 = c_7 |\log_{10}(\mathrm{SNR} - c_8)^{c_9}| + c_{10} \tag{18}$$

where c_i, $i = [7, 10]$ are additional coefficients determined empirically via curve fitting.

The final empirical model of the information beamwidth is thus given by

$$\begin{aligned}\mathrm{IB} &= \mathrm{IB}_1 \times \mathrm{IB}_2 \\ &= [c_1 e^{c_2 a} + c_3][c_4 e^{c_5 d} + c_6][c_7 |\log_{10}(\mathrm{SNR} - c_8)^{c_9}| + c_{10}]\end{aligned} \tag{19}$$

For each surface generated, multiple algorithms were used to extract coefficients to fit the model, including the Levenberg-Marquardt and the trust-region reflection [26], [27] and two robustness methods, least absolute residuals and bisquare residuals [28], [29]. The RMS error of the models were then compared to the surfaces for each QAM order. The parameters of (19) resulting from the model fit are given in Table II, and the error between the model and the simulated ideal information beamwidth are given in Table III. The total RMS error in estimating the information beamwidth using the model (19) is less than $1.3°$. In addition to the RMSE analysis, we evaluated the maximum error. For amplitude ratios greater than 2 dB, the maximum model error was less than $3°$; for amplitude ratios between 12 dB and 15 dB, the maximum error was less than $1°$. Fig. 9 (c) demonstrates that (19) provides good agreement between the model and simulation results for 8-QAM.

VI. Conclusion

Dynamically switching the input signal feeds with only amplitude changes in a two-element array yields sufficient phase dynamics to support directional modulation while negligibly impacting the magnitude pattern. For low amplitude ratios (6 dB or 12 dB) the array gain is minimally impacted while the information beamwidth is significantly narrowed compared to a traditional 0 dB amplitude ratio case. We analyzed the theoretical impact of dynamic amplitude weighting and showed through theory and measurement that it can be interpreted as dynamic motion of the array phase center. This provides a physical interpretation of the mechanics of the subsequent directional modulation that can be useful in a design procedure. Furthermore, the information beamwidth model can be used as a design guideline to

determine desired amplitude weights for given modulation orders. Used in a dynamic array, the differential phase pattern resulting from the motion of the phase center yields a narrow information beam that is the result of the array dynamics, and not low SNR. Since the presented amplitude modulation can be implemented separately from traditional phased array weighting, the information beam can be steered using standard phased array beamsteering approaches. This work demonstrated the concept using a simple two-element array as a proof-of-concept; however, the technique should be applicable to larger arrays as well.

REFERENCES

[1] M. P. Daly and J. T. Bernhard, "Directional modulation technique for phased arrays," *IEEE Transactions on Antennas and Propagation*, vol. 57, no. 9, pp. 2633–2640, 2009.

[2] M. P. Daly, E. L. Daly, and J. T. Bernhard, "Demonstration of directional modulation using a phased array," *IEEE Transactions on Antennas and Propagation*, vol. 58, no. 5, pp. 1545–1550, 2010.

[3] M. P. Daly and J. T. Bernhard, "Beamsteering in pattern reconfigurable arrays using directional modulation," *IEEE Transactions on Antennas and Propagation*, vol. 58, no. 7, pp. 2259–2265, 2010.

[4] N. Valliappan, A. Lozano, and R. W. Heath, "Antenna subset modulation for secure millimeter-wave wireless communication," *IEEE Transactions on Communications*, vol. 61, no. 8, pp. 3231–3245, 2013.

[5] B. You, I.-H. Lee, and H. Jung, "Exact secrecy rate analysis of antenna subset modulation schemes," *IEEE Systems Journal*, vol. 15, no. 4, pp. 4827–4830, 2021.

[6] E. Baghdady, "Directional signal modulation by means of switched spaced antennas," *IEEE Transactions on Communications*, vol. 38, no. 4, pp. 399–403, 1990.

[7] B. Guo, Y.-h. Yang, G. Xin, and Y.-q. Tang, "Combinatorial interference directional modulation for physical layer security transmission," in *2016 IEEE Information Technology, Networking, Electronic and Automation Control Conference*, 2016, pp. 710–713.

[8] Y. Ding and V. F. Fusco, "A vector approach for the analysis and synthesis of directional modulation transmitters," *IEEE Transactions on Antennas and Propagation*, vol. 62, no. 1, pp. 361–370, 2014.

[9] A. Babakhani, D. B. Rutledge, and A. Hajimiri, "Transmitter architectures based on near-field direct antenna modulation," *IEEE Journal of Solid-State Circuits*, vol. 43, no. 12, pp. 2674–2692, 2008.

[10] S. M. Ellison, J. M. Merlo, and J. A. Nanzer, "Distributed antenna array dynamics for secure wireless communication," *IEEE Transactions on Antennas and Propagation*, vol. 70, no. 4, pp. 2740–2749, 2022.

[11] A. A. Arisheh, J. M. Merlo, and J. A. Nanzer, "Design of a single-element dynamic antenna for secure wireless applications," *IEEE Transactions on Antennas and Propagation*, pp. 1–1, 2023.

[12] A. Narbudowicz, A. Zandamela, N. Marchetti, and M. J. Ammann, "Energy-efficient dynamic directional modulation with electrically small antennas," *IEEE Antennas and Wireless Propagation Letters*, vol. 21, no. 4, pp. 681–684, 2022.

[13] A. Zandamela, N. Marchetti, and A. Narbudowicz, "Directional modulation from a wrist-wearable compact antenna," in *2022 16th European Conference on Antennas and Propagation (EuCAP)*, 2022, pp. 1–5.

[14] A. Kumar, A. D. Sarma, E. Ansari, and K. Yedukondalu, "Improved phase center estimation for gnss patch antenna," *IEEE Transactions on Antennas and Propagation*, vol. 61, no. 4, pp. 1909–1915, 2013.

[15] J. R. Randall, A. A. Arisheh, J. M. Merlo, and J. A. Nanzer, "A dynamic array using spatial amplitude modulation with an asymmetric wilkinson power divider for secure wireless applications," *IEEE Antennas and Wireless Propagation Letters*, pp. 1–5, 2023.

[16] C. A. Balanis, *Antenna theory: analysis and design*. Wiley-Interscience, 2005.

[17] D. Carter, "Phase centers of microwave antennas," *IRE Transactions on Antennas and Propagation*, vol. 4, no. 4, pp. 597–600, 1956.

[18] E. Muehldorf, "The phase center of horn antennas," *IEEE Transactions on Antennas and Propagation*, vol. 18, no. 6, pp. 753–760, 1970.

[19] H. Mathis, "A short proof that an isotropic antenna is impossible," *PROCEEDINGS OF THE INSTITUTE OF RADIO ENGINEERS*, vol. 39, no. 8, pp. 970–970, 1951.

[20] M. Teichman, "Determination of horn antenna phase centers by edge diffraction theory," *IEEE Transactions on Aerospace and Electronic Systems*, vol. AES-9, no. 6, pp. 875–882, 1973.

[21] Y. Hu, "A method of determining phase centers and its application to electromagnetic horns," *Journal of the Franklin Institute*, vol. 271, no. 1, pp. 31–39, 1961. [Online]. Available: https://www.sciencedirect.com/science/article/pii/S0016003261910134

[22] L. Ying, T. Wei, and Z. Xin, "Research on the high precise calibration of the gps receiving antenna phase center," in *Proceedings of the 9th International Symposium on Antennas, Propagation and EM Theory*, 2010, pp. 4–7.

[23] T. Hertel, "Phase center measurements based on the three-antenna method," in *IEEE Antennas and Propagation Society International Symposium. Digest. Held in conjunction with: USNC/CNC/URSI North American Radio Sci. Meeting (Cat. No.03CH37450)*, vol. 3, 2003, pp. 816–819 vol.3.

[24] J. Yang, "Calculation of the phase center of an ultra-wideband feed for reflector antennas," in *2013 Proceedings of the International Symposium on Antennas Propagation*, vol. 01, 2013, pp. 30–32.

[25] J. Tuovinen, A. Lehto, and A. Raisanen, "A novel differential phase method to measure phase pattern and phase center of a horn antenna at 110 ghz," in *International Symposium on Antennas and Propagation Society, Merging Technologies for the 90's*, 1990, pp. 1298–1301 vol.3.

[26] K. Levenberg, "A method for the solution of certain non-linear problems in least squares," *Quarterly of applied mathematics*, vol. 2, no. 2, pp. 164–168, 1944.

[27] D. C. Sorensen, "Newton's method with a model trust region modification," *SIAM Journal on Numerical Analysis*, vol. 19, no. 2, pp. 409–426, 1982.

[28] E. Schlossmacher, "An iterative technique for absolute deviations curve fitting," *Journal of the American Statistical Association*, vol. 68, no. 344, pp. 857–859, 1973.

[29] M. M. Fouad, R. M. Dansereau, and A. D. Whitehead, "Image registration under local illumination variations using robust bisquare m-estimation," in *2010 IEEE International Conference on Image Processing*, 2010, pp. 917–920.

Jacob R. Randall received the B.S. degree in electrical engineering from Michigan State University, East Lansing, in 2020. From 2019-2020, Jacob was the electrical team manager for the Michigan State University Solar Racing team. He worked as an EMI and power electronics engineer for aerospace applications from 2020-2021. He is currently pursuing the Ph.D. degree at Michigan State University, where his research interests include dynamic distributed antennas and radar detection and tracking for automotive, aerospace, and defense applications. Jacob won second place in the Student Design Contest at the 2020 IEEE International Symposium on Antennas and Propagation.

Amer Abu Arisheh (Graduate Student Member, IEEE) received the BS.c. degree in Electrical Engineering from The University of Jordan, Amman, Jordan and his MS.c. degree in Electrical Engineering/Wireless Communications from Jordan University of Science and Technology, Irbid, Jordan. He is currently pursuing the Ph.D. degree in electrical engineering at Michigan State University, East Lansing, MI, USA. His research interests include dynamic antennas and fundamental electromagnetics.

Jason M. Merlo (Graduate Student Member, IEEE) received the B.S. degree in computer engineering from Michigan State University, East Lansing, MI, USA in 2018, where he is currently pursuing the Ph.D. degree in electrical engineering. From 2017-2021 he was project manager and electrical systems team lead of the Michigan State University AutoDrive Challenge team. His current research interests include distributed radar and wireless system synchronization, interferometric arrays, synthetic aperture radar, joint radar-communications, and automotive/automated vehicle radar applications. Jason was the recipient of a 2023 URSI Young Scientist Award and a 2023 IEEE MTT-S Graduate Fellowship. He won first place in the Student Paper Competition at the 2023 IEEE International Microwave Symposium and won Honorable Mention in the Student Paper Contest at the 2023 IEEE International Symposium on Antennas and Propagation. He won Second Place in the Student Design Contest at the 2020 IEEE International Symposium on Antennas and Propagation and was a finalist in the Student Safety Technology Design Competition at the 2017 International Technical Conference on Enhanced Safety of Vehicles.

Jeffrey A. Nanzer (S'02–M'08–SM'14) received the B.S. degrees in electrical engineering and in computer engineering from Michigan State University, East Lansing, MI, USA, in 2003, and the M.S. and Ph.D. degrees in electrical engineering from The University of Texas at Austin, Austin, TX, USA, in 2005 and 2008, respectively.

From 2008 to 2009 he was with the University of Texas Applied Research Laboratories in Austin, Texas as a Post-Doctoral Fellow designing electrically small HF antennas and communications systems. From 2009 to 2016 he was with the Johns Hopkins University Applied Physics Laboratory where he created and led the Advanced Microwave and Millimeter-Wave Technology Section. In 2016 he joined the Department of Electrical and Computer Engineering at Michigan State University where he held the Dennis P. Nyquist Assistant Professorship from 2016 through 2021. He is currently an Associate Professor. He directs MSU's Electromagnetics Laboratory, which consists of the Antenna Laboratory, the Radar Laboratory, and the Wireless Laboratory. He has published more than 200 refereed journal and conference papers, two book chapters, and the book Microwave and Millimeter-Wave Remote Sensing for Security Applications (Artech House, 2012). His research interests are in the areas of distributed phased arrays, dynamic antenna arrays, millimeter-wave imaging, remote sensing, millimeter-wave photonics, and electromagnetics.

Dr. Nanzer is a Distinguished Microwave Lecturer for the IEEE Microwave Theory and Techniques Society (Tatsuo Itoh Class of 2022-2024). He was a Guest Editor of the Special Issue on Special Issue on Radar and Microwave Sensor Systems in the IEEE Microwave and Wireless Components Letters in 2022. He is a member of the IEEE Antennas and Propagation Society Education Committee and the USNC/URSI Commission B, was a founding member and the First Treasurer of the IEEE APS/MTT-S Central Texas Chapter, served as the Vice Chair for the IEEE Antenna Standards Committee from 2013 to 2015, and served as the Chair of the Microwave Systems Technical Committee (MTT-16), IEEE Microwave Theory and Techniques Society from 2016 to 2018. He was a recipient of the Google Research Scholar Award in 2022 and 2023, the IEEE MTT-S Outstanding Young Engineer Award in 2019, the DARPA Director's Fellowship in 2019, the National Science Foundation (NSF) CAREER Award in 2018, the DARPA Young Faculty Award in 2017, and the JHU/APL Outstanding Professional Book Award in 2012. He and his students have received several best paper awards, including first place in the student paper competition at the 2023 IEEE 2023 International Microwave Symposium, second place at the 2020 IEEE International Symposium on Antennas and Propagation, and honorable mention at the 2023 IEEE International Symposium on Antennas and Propagation. He is currently an Associate Editor of the IEEE TRANSACTIONS ON ANTENNAS AND PROPAGATION.